Stimulated Brillouin Scattering in Multispecies Laser-Produced Plasmas

P. E. Young and M. E. Foord
Lawrence Livermore National Laboratory, University of California, P.O. Box 808, Livermore, California 94551

A. V. Maximov and W. Rozmus
Department of Physics, Theoretical Physics Institute, University of Alberta, Edmonton, Alberta, Canada T6G 2J1
(Received 6 February 1996)

Growth and saturation of the stimulated Brillouin scattering (SBS) instability has been studied in C, CH, and CH_2 laser-produced plasmas which have nearly identical density profiles. The backscattered reflectivity is highest for the CH_2 plasma ($\sim$15%) and up to $\sim$5 times lower for the pure carbon plasma. This result is explained by the stationary inhomogeneous theory of SBS and confirmed by numerical simulations provided one allows for the nonuniform expansion of hydrogen and carbon ions that leads to an axial asymmetry of the SBS gain and results in the observation of a blueshifted scattered light spectrum from CH targets. [S0031-9007(96)00909-X]

PACS numbers: 52.35.Nx, 52.40.Nk, 52.50.Jm

The stimulated Brillouin scattering (SBS) instability is produced by the parametric coupling of an incident light wave to an ion acoustic wave and a scattered light wave whose frequency is within a percent of the incident laser frequency, ω_0 [1,2]. The SBS instability is of concern in inertial confinement fusion (ICF) applications because of the potential of scattering a large percentage of the incident laser light in the underdense corona, decreasing the coupling efficiency of the laser to the imploding target. Recent work on gasbag and simple *Hohlraum* [3] targets have shown that in ICF plasmas with more than one species of ions it is important to include all the species in the modeling in order to understand the Landau damping of the ion waves [3–7] and the effect of this on SBS. In this work we show that in the flowing multispecies plasmas characteristic of both directly driven and indirectly driven ICF, the mean-ion model is inadequate for quite another reason. We find that SBS is strongly affected by the separation of the ion species due to differential ion flow in the ambipolar fields of the expanding plasma, a result which successfully models the previously unexplained observed broadening towards shorter wavelength of SBS spectra from plasmas created from plastic foils [8,9].

In this Letter, we describe an experiment in which a focused laser beam interacts with underdense plasmas preformed with C, CH, and CH_2 target materials. The target thicknesses have been chosen so that the laser pulse always interacts with virtually the same electron density profile independent of target material. The backscatter spectra from the C targets are symmetric about the central plasma ion acoustic frequency, while those from the CH and CH_2 targets are asymmetrically broadened towards shorter wavelengths, producing reflectivities up to 5 times higher than those from the C targets. Analytic analysis of the convective SBS gain shows that the observed asymmetry is a result of the differential flow velocities of the H and C ions which produce gradients in the sound speed that enhance (reduce) the gain on the front (rear) side of the target. The predictions of a one-dimensional (1D) fully nonlinear fluid model of SBS, which accounts for nonuniform profiles of flow velocity, plasma density, and ion concentration, are consistent with the experimental results.

The experiment was conducted using the Janus laser at Lawrence Livermore National Laboratory. The targets used were foils: 45 μgm/cm^2 carbon, 50 μgm/cm^2 parylene (CH), and 50 μgm/cm^2 polypropylene (CH_2). The target thicknesses were chosen so the targets would have the same column density, and therefore produce the same electron density profile, regardless of the target material. The plasma was formed by a 50 J, 0.532 μm wavelength, 1 ns nominally square pulse focused on target to a spot diameter of 400 μm. At a time of 1.5 ns after the end of the plasma forming pulse, a 1.064 μm wavelength, 100 ps full width at half maximum (FWHM) Gaussian pulse arrived at the target. The best focus of this second beam was located at the target plane and had a FWHM diameter of 9 μm; because the spatial profile of the beam at best focus is non-Gaussian [10], the diameter which contains half the energy is 16 μm which gives a peak intensity of 5×10^{16} W/cm^2. The confocal parameter was approximately 200 μm. The time interval between the two beams was chosen so that the peak density seen by the second beam was high enough to observe saturation while keeping the reflected SBS energy high enough to observe the exponential growth of the instability. Throughout the experiment, best focus was always at the target plane and the intensity was changed by varying the energy.

The density profile was measured using a folded-wave interferometer that used a 0.35 μm wavelength, 50 ps probe pulse that arrives at the target at the peak of the 100 ps interaction pulse. The interferogram was recorded using a television camera, then Abel inverted to produce axial density profiles. Figure 1 shows typical axial density

 0031-9007/96/77(7)/1278(4)$10.00

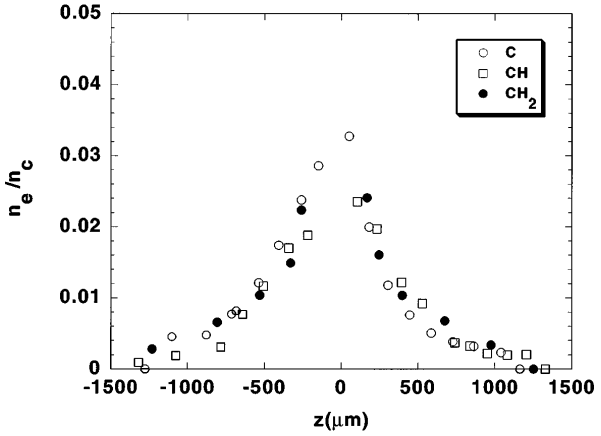

FIG. 1. Measured axial density profiles for the three target materials.

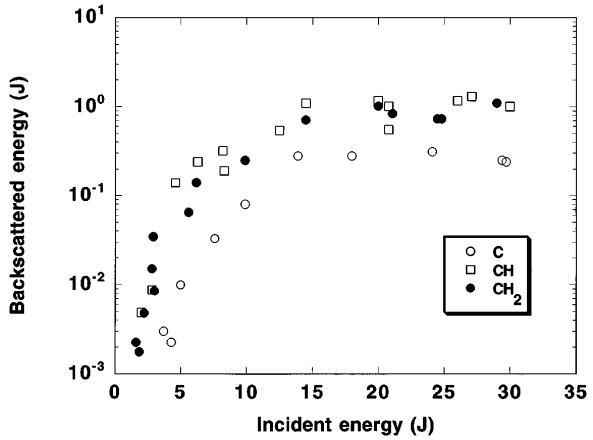

FIG. 2. Scaling of the backscattered SBS reflected energy (J) as a function of incident laser energy (J) and target material. At the highest incident energies, carbon has the lowest reflectivity.

profiles for C, CH, and CH_2 targets. The profiles are virtually identical, with a peak density near $0.025 n_c$ where n_c is the critical density at which the plasma frequency equals ω_0. The foil is initially located at $z = 0$. For densities this low, the filamentation instability has been shown experimentally and theoretically to be below threshold [10].

The energy and spectrum of the backscattered light near the laser wavelength were monitored as the laser energy was varied. A whole-beam beam splitter reflected 4% of the light backscattered into the focusing lens to a calorimeter which measures the backscattered energy. The light was collected at three angles: 180°, 135°, and 45° relative to the direction of propagation of the interaction beam, and multiplexed using optical fibers at the input of a 1.25 m Czerny-Turner spectrometer and recorded using a streak camera with an S-1 photocathode and ~100 ps time resolution. The main purpose of the streak camera for the experiment discussed here was to separate out the signals from different angles. We verified that the collected light energies were too low to produce spectral broadening in the optical fiber. We observed that the mixed species plasmas, CH and CH_2, have reflectivities up to 5 times that of the carbon plasma at the highest laser energy. In Fig. 2, we plot the backscattered energy as a function of incident laser energy by integrating the streaked signal for each event. The streak signal is calibrated at the highest energies by the calorimeter measurements. The energy exhibits exponential growth up to an intensity of 1.5×10^{15} W/cm^2. Further increase in the incident laser intensity leads to an approximately constant backscattered signal level which indicates saturation of the instability.

The higher reflectivity of the mixed species plasmas is a result of a spectral broadening not observed with the carbon plasma. The carbon plasma shows a spectrum (see Fig. 3) that has a redshifted peak and a bandwidth of about 20 Å, independent of the incident laser energy. The mixed species plasmas, on the other hand, show a similar spectrum only at lower energies; as the laser energies are increased, the spectrum becomes broader, mainly towards the blue. Note that the reflectivity at $\lambda = 10\,650$ Å, does not change very much. The drop in signal at $\lambda = 10\,665$ Å is an instrumental cutoff.

We interpret the redshifted peak observed in the carbon plasmas for all laser energies, and in the mixed-species plasmas at low laser energies as due to SBS growing at the peak of the plasma profile. This is a region where we expect SBS to grow fastest because the density gradient scale length is very large. From the SBS frequency matching conditions, the frequency shift of the scattered electromagnetic wave (of frequency ω_s) is $\Delta\omega = \omega_0 - \omega_s = \omega_{ia}$. The ion acoustic frequency of the fast mode, ω_{ia}, and wave vector, $\mathbf{k}_{ia}$, satisfy the linear dispersion relation

$$\sum_\alpha \frac{Z_\alpha^2 n_\alpha T_e}{n_e m_\alpha} \frac{k_{ia}^2}{(\omega_{ia} - \mathbf{k}_{ia} \cdot \mathbf{u}_\alpha)^2} = 1\,, \qquad (1)$$

where Z_α, n_α, m_α, and $\mathbf{u}_\alpha$ are the charge, density, mass, and flow velocity of each ion species [$\alpha = 1$ (carbon),

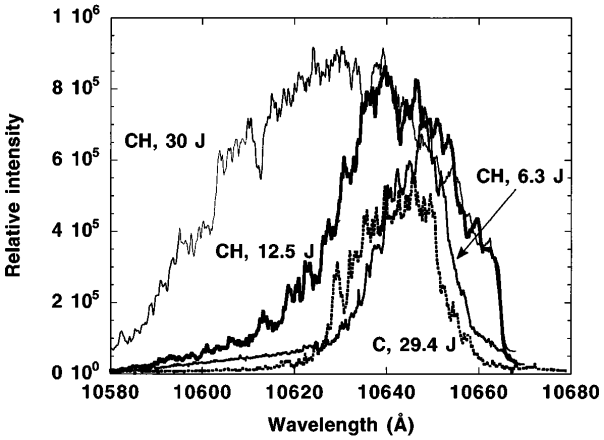

FIG. 3. Behavior of the CH backscattered spectrum as a function of the incident energy. The evolution of the spectrum is further illustrated by lineouts of the streaked spectra at the peak of the laser pulse.

2 (hydrogen)], respectively. The ion thermal effects in Eq. (1) have been neglected. Close to the peak of the density profile, where flow velocities are small as compared to the sound speed, one obtains from Eq. (1),

$$\omega_{ia} = k_{ia} c_s + \mathbf{k}_{ia} \cdot \mathbf{u}\,, \tag{2}$$

where $c_s = (\sum_\alpha Z_\alpha^2 n_\alpha T_e / n_e m_\alpha)^{1/2}$ is the sound speed, and $\mathbf{u} = (\sum_\alpha Z_\alpha^2 n_\alpha \mathbf{u}_\alpha / m_\alpha)/(\sum_\alpha Z_\alpha^2 n_\alpha / m_\alpha)$ is the flow velocity. Note that Eq. (2) is also an approximate solution to the dispersion relation (1) in the limit of $|\mathbf{u}_1 - \mathbf{u}_2| \ll c_s$. Since $u \approx 0$ at the top of the plasma profile, Eq. (2) predicts redshifted scattered light which should be weakly dependent on the observation angle. This is confirmed by the spectrum observed at 135° which shows similar redshift. From this interpretation, we obtain an estimate of the electron temperature of 500 eV.

Since the hydrogen ions will expand faster than the carbon ions, it is possible to obtain regions of plasma where there is a larger concentration of hydrogen ions than carbon ions. The self-similar expansion of a two species plasma was examined analytically by Gurevich [11] who showed this effect for the first time. In Fig. 4 we display inhomogeneous profiles of plasma parameters used in numerical simulations of SBS. They have been obtained from the numerical solutions to the fluid model which describes expansion of the exploding foil target. The background electron density $n_e(z)$ at $t = 1$ ns approximately corresponds to the experimental density profile shown in Fig. 1 for the temperature $T_e = 500$ eV. Figure 4 shows the symmetric density profiles and part of the antisymmetric axial velocity profiles. The laser propagates from the left to right. The hydrogen ion concentration increases away from the center of the target and dominates for $z > 200$ μm. The large values of flow velocities u, u_1 (carbon), and u_2 (hydrogen) normalized to $c_s(0)$ (the value of c_s at $z = 0$) are responsible for the blueshifted SBS light (cf. Fig. 3). The spatial scales shown in Fig. 4 are consistent with Gurevich's [11] solutions.

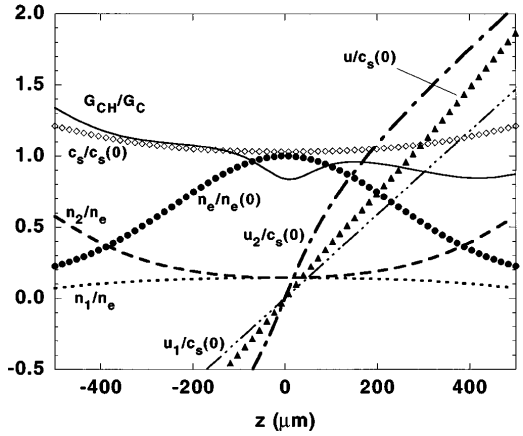

FIG. 4. Typical profiles of electron density $n_e/n_e(0)$, carbon ion, n_1/n_e, and hydrogen ion, n_2/n_e, concentrations, axial plasma flow velocity, $u/c_s(0)$, sound speed, $c_s/c_s(0)$, and axial flow velocities of carbon, $u_1/c_s(0)$, and hydrogen, $u_2/c_s(0)$, used in SBS simulations. The curve marked $G_{\mathrm{CH}}/G_{\mathrm{C}}$ shows the ratio of SBS gains for CH and C targets calculated from Eq. (3).

The SBS was modeled using a one-dimensional, fully nonlinear fluid description [12] which was generalized to account for a second ion species, inhomogeneous plasma flow and density, and Landau damping. This wave interaction code describes SBS in a plasma with background conditions (n_α, u_α, $\alpha = 1, 2$) shown in Fig. 4. In the simulations, the plasma extends over the length of $L = 1000$ μm with the point of the initial target location at $z = 0$ μm. This point is characterized by $u_\alpha = 0$ and an equal concentration of carbon and hydrogen ions, $n_1 = n_2$, for CH targets. Within the length L, the electron density varies from its maximum value $n_e = 0.03 n_c$ at $z = 0$ μm to $n_e \approx 0.01 n_c$ at the left boundary. Figure 5 shows examples of backscattered light spectra obtained from numerical simulations. The mixed ion target shows higher reflectivity by a factor up to two, 24% as compared to 13% for the carbon target. The main reason for this increase is a broader spectrum of SBS light from CH plasmas. The high intensity examples from Fig. 5 represent a moderate laser flux of 7.5×10^{14} W/cm^2, giving rise to processes which could be understood within linear theory of SBS. The lower intensity result (5×10^{14} W/cm^2) from the CH target is mostly redshifted and quite narrow, consistent with experimental results.

In our code, the nonlinear physics of large amplitude sound waves includes all previously described mechanisms within the fluid approximation, i.e., frequency shift, harmonic generation, and localization of sound waves [13]. At high intensities, these mechanisms can contribute to broadening of scattered light spectra due to rapid time variations of SBS reflectivity. We have found, however, that the spectral width associated with this effect is much smaller than the width observed in experiments or the spectral width produced in simulations due to inhomogeneities of plasma parameters. Therefore, the essential processes responsible for larger SBS reflectivity in mixed ion species

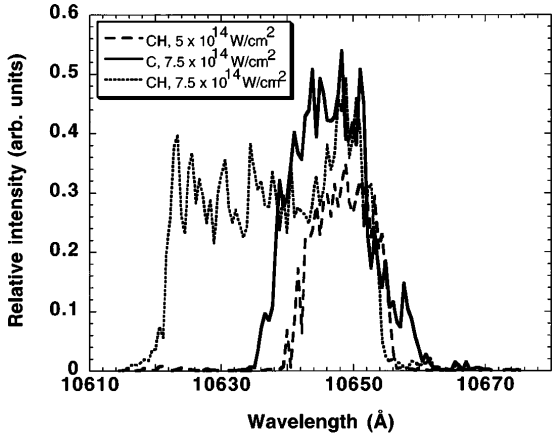

FIG. 5. Spectra of SBS scattered light for the plasma profiles shown in Fig. 4 for different targets and laser intensities.

targets can be qualitatively described using linear stationary theory of SBS in inhomogeneous plasmas.

In order to connect to analytic theory, we consider a convective growth of SBS for the case of laser wave vector k_0 along the z axis parallel to both density and flow velocity gradients. According to convective theory, the instability grows by e^G where the convective gain G is given by [9,14,15] $G = 2\pi\gamma_0^2/|\kappa_z' v_{ia,z} v_{s,z}|$, where γ_0 is the homogeneous growth rate and $v_{ia,z}$ and $v_{s,z}$ are z components (normal to the target) of ion acoustic wave and scattered light group velocities, respectively. The wave vector mismatch κ' in G is given by [14] $\kappa_z' = dk_{0,z}/dz - dk_{ia,z}/dz - dk_{s,z}/dz$, where the subscript z denotes the component of the wave vectors of the pump wave, k_0, resonant ion acoustic wave, k_{ia}, and the scattered light wave, k_s, in the z direction. We find that

$$G \simeq \frac{2\pi\gamma_0^2}{\omega_0 |\sin^2(\theta/2)\cos\theta D|}, \tag{3}$$

where $D = (n_e/n_c)[-u - c_s\sin(\theta/2)]/L_N\cos\theta + 2(1 - n_e/n_c)c_s[1/L_u + 1/\sin(\theta/2)L_c]$. The gradient scale lengths L_u, L_c, and L_N are defined as $L_u = c_s(du/dz)^{-1}$, $L_c = c_s(dc_s/dz)^{-1}$, $L_N = n_e(dn_e/dz)^{-1}$, and u is the z component of the flow velocity $\mathbf{u}$.

The analytic expression (3) illustrates two important effects. One can see from the linear dispersion relation (1) that the ion acoustic wave frequency depends on the ion concentration. This dependence leads to a broader scattered electromagnetic wave spectrum, because a wider range of ion acoustic frequencies can satisfy local SBS matching conditions in plasmas with nonuniform distribution of different species. The broader spectrum for CH targets in Fig. 5 is due to the contribution from the flow velocity of the hydrogen ions to ω_{ia} [Eq. (2)], which changes over a wider range of values than the carbon flow velocity, and due to the varying ion concentration.

The second important effect of multi-ion species targets is the dependence of the sound speed c_s on z due to the varying concentration of hydrogen and carbon ions. The c_s gradient can contribute to the expression for the SBS gain G (3), through the scale length L_c. The factor D in (3) describes dependence of the SBS gain on L_c and L_u and the dependence on the electron density inhomogeneity L_N, which is weaker by a factor n_e/n_c. For backscattered SBS and $n_e/n_c \ll 1$ the expression for D can be simplified to the following form $D \approx 2c_s(1/L_c + 1/L_u)$. The simplified form of D explains the observed asymmetry towards blue wavelengths in the spectrum of the scattered light from CH targets (cf. Figs. 3 and 5). From the curves depicting $u/c_s(0)$ and $c_s/c_s(0)$ in Fig. 3, one can see that in front of the target ($z < 0$), L_c is negative and reduces the mismatch due to the inhomogeneity of the flow, L_u, while in the back of the target ($z > 0$) both L_c and L_u are positive which increases D and reduces the gain. This is also illustrated by the curve showing the ratio of SBS gains for CH and C targets, G_{CH}/G_C calculated locally from Eq. (3) for backscattered light. The asymmetry of this line is due to the asymmetry of G_{CH} produced by the effect described above. Over 30% difference in gain amounts to more than an order of magnitude larger amplification for SBS from CH plasma in front of the target. It is also likely that at higher reflectivities pump depletion may localize SBS growth in front of the target where it leads to blueshifted scattered light. Note that the z variation of the frequency shift ω_{ia} (2) is defined by the flow velocity $u(z)$ and is only weakly affected by the changes in c_s due to varying concentrations of ions for the parameters of our experiment.

In summary, we have shown that, although theory and experiment have shown the importance of mixed ion species to the damping of SBS, in laser-produced plasmas, the hydrodynamic expansion produces a situation in which a mixed species plasma results in a higher SBS reflectivity than a single species plasma. The experimental results have been successfully modeled by a fully nonlinear fluid code.

We acknowledge useful discussions with A. Rubenchik and G. Guethlein. We thank W. Cowens, R. Gonzales, and G. London for operating the Janus laser during the experiment. This work was performed under the auspices of the U.S. Department of Energy by the Lawrence Livermore National Laboratory under Contract No. W-7405-Eng-48. A. V. M. and W. R. acknowledge support from the Natural Sciences and Engineering Research Council of Canada.

[1] M. V. Goldman and D. F. DuBois, Ann. Phys. (N.Y.) **38**, 117 (1966).
[2] J. F. Drake *et al.*, Phys. Fluids **17**, 778 (1974).
[3] S. C. Wilks *et al.*, Phys. Rev. Lett. **74**, 5048 (1995); J. C. Fernandez *et al.*, Phys. Rev. E **53**, 2747 (1996).
[4] B. D. Fried and R. W. Gould, Phys. Fluids **4**, 139 (1961); B. D. Fried *et al.*, Phys. Fluids **14**, 2388 (1971).
[5] I. Alexeff *et al.*, Phys. Rev. Lett. **19**, 422 (1967).
[6] C. E. Clayton *et al.*, Phys. Fluids **24**, 2312 (1981).
[7] H. X. Vu *et al.*, Phys. Plasmas **1**, 3542 (1994); E. A. Williams *et al.*, Phys. Plasmas **2**, 129 (1995).
[8] D. W. Phillion *et al.*, Phys. Rev. Lett. **39**, 1529 (1977); K. Tanaka *et al.*, Phys. Fluids **27**, 2960 (1984); K. Tanaka *et al.*, Phys. Fluids **28**, 2910 (1985); A. N. Mostovych *et al.*, Phys. Rev. Lett. **59**, 1193 (1987).
[9] P. E. Young *et al.*, Phys. Fluids **2**, 1907 (1990).
[10] P. E. Young *et al.*, Phys. Plasmas **2**, 2825 (1995).
[11] A. V. Gurevich *et al.*, Zh. Eksp. Teor. Fiz. **63**, 516 (1972) [Sov. Phys. JETP **36**, 274 (1973)].
[12] J. Candy *et al.*, Phys. Rev. Lett. **65**, 1889 (1990).
[13] W. Rozmus *et al.*, Phys. Fluids B **4**, 576 (1992); S. Huller, Phys. Fluids B **3**, 3317 (1991); M. Casanova *et al.*, Phys. Rev. Lett. **54**, 2230 (1985); J. A. Heikkinen *et al.*, Phys. Fluids **27**, 707 (1984); V. P. Silin and V. T. Tikhonchuk, Sov. Phys. JETP **56**, 765 (1982).
[14] M. N. Rosenbluth, Phys. Rev. Lett. **29**, 565 (1972).
[15] C. S. Liu *et al.*, Phys. Rev. Lett. **31**, 697 (1973); Phys. Fluids **17**, 1211 (1974).